Mechanical Systems and Signal Processing 84 (2017) 598–614

Contents lists available at ScienceDirect

Mechanical Systems and Signal Processing

journal homepage: www.elsevier.com/locate/ymssp

Development of a scientific torsional system experiment containing controlled single or dual-clearance non-linearities: Examination of step-responses

Michael D. Krak, Rajendra Singh *

Acoustics and Dynamics Laboratory, NSF Smart Vehicle Concepts Center, Department of Mechanical and Aerospace Engineering, The Ohio State University, Columbus, OH 43210, USA

ARTICLE INFO

Article history:
Received 15 February 2016
Received in revised form
21 June 2016
Accepted 17 July 2016

Keywords:
Experimental dynamics
Vibro-impacts
Clearance non-linearity
Non-linear system modeling

ABSTRACT

The chief goal of this paper is to propose a new laboratory experiment that exhibits the step-response of a torsional system containing one or two controlled clearances. This work is motivated by the disadvantages of prior large-scale experiments which utilize production vehicle drivelines and their components with significant real-life complexities. The conceptual and physical design features, which include sizing, modal properties, excitation, and instrumentation, are discussed with the goal of creating a controlled experiment. Like prior literature, a step-down torque excitation is selected and all analyses are performed on the acceleration signals to observe vibro-impact in the time domain. Typical measurements (for both the single and dual-clearance configurations) exhibit rich non-linear behavior, including the double-sided impact regime and a time-varying oscillatory period. Additionally, new measurements are compared to predictions from simple reduced order non-linear models to verify the feasibility of the proposed experiment. Finally, the utility of this experiment is demonstrated by comparing its measurements to a prior large-scale experiment that accommodates a production vehicle clutch damper with multiple stages. The hardening and softening effects in both experiments are discussed in the context of double and single-sided impacts as well as the oscillatory periods that vary with time.

1. Introduction

Most torsional systems in vehicles and machinery contain one or more discontinuous non-linear features by design or otherwise [1–9]. Such non-linear elements include clearances (e.g. backlashes between gears), multi-staged torsional springs, pre-load and stopper features (e.g. torque transmission devices), and multi-staged dry friction components. Of this group, the clearance or gap element is the most fundamental as it is required to assemble components without interference while providing space for lubrication. Presence of such clearances in multi-degree of freedom systems induce conditions for vibro-impact phenomena, depending on the value of mean and alternating loads. Gear rattle [4,9,10] and vehicle driveline clunk [4–8] are common physical manifestations of such systems as evident from many noise and vibration issues in the ground vehicle industry. While several researchers have developed non-linear simulation models, they often include many

* Corresponding author.
E-mail address: singh.3@osu.edu (R. Singh).

http://dx.doi.org/10.1016/j.ymssp.2016.07.026
0888-3270/

simplifications and/or incorporate assumed or empirical parameters. There is clearly a need for a scientific experiment that could yield physical insight, accurate parameters, and benchmark time domain data for the validation of non-linear simulation models. Therefore, it is the chief goal of this article and as such a new laboratory experiment with controlled clearance element(s), while being distinctly different from the prior experimental studies [4–8], will be proposed.

2. Problem formulation

Couderc et al. [4] proposed a system-level rotating experiment to better understand gear rattle during engine run-up. Their experiment accommodates several production components, such as a clutch damper and vehicle transmission, while containing several clearances spread across multiple locations. Likewise, a different type of experiment must be considered to study vehicle driveline clunk, typically induced by a sudden change in the mean operating point of the driveline (often known as a tip-in or tip-out event) [4–8]. The simplest way to implement such excitation in a laboratory setting is to apply a step-down torque under vibratory conditions, which is essentially free vibration about a static equilibrium. Few system-level experiments that employ the step-response method have been proposed in the literature [5–7]. Common features across all test rigs [5–7] include the following: i) Production vehicle driveline components are often utilized; ii) The systems are made positive-definite to achieve vibratory conditions (i.e. at least one torsional component is fixed to ground); iii) Two or more clearance elements are present; and iv) A step-down torque is applied via a variable mass-drop from a torsion arm. Although these experiments [5–7] provide much needed system-level insight, it is also necessary to study non-linear dynamics at the component-level. For example, consider the experiment recently proposed by Krak et al. [8], which has been developed to provide parameter estimation for a clutch damper under dynamic conditions. This particular experiment [8] accommodates one or two production clutch dampers and is excited by a step-like torque like the clunk experiments [5–7]; however, the external torque is supplied by a pneumatic actuator rather than a mass-drop due to the relatively high torque capacity of the device.

These aforementioned large-scale experiments [4–8] have the following intrinsic benefits: i) Interactions between multiple non-linear features are maintained; ii) System and component-level dynamics can be studied under realistic boundary conditions; iii) Real-world type excitation is more easily achieved; and iv) Parameter estimation has greater fidelity [11]. However, there are also several inherent disadvantages, such as increased cost (e.g. labor, hardware, instrumentation, and laboratory space), a higher degree of complexity, and, most important, a lack of controllability. The latter two are largely due to the use of production components, which can contain multiple (known and unknown) non-linear features while being subject to variations in assembly and manufacturing. Therefore, the goal of this paper is to address this critical need by proposing a more controlled and scientific version of prior large-scale experiments [5–8]. Accordingly, the following specific objectives are defined: 1) Develop a new controlled laboratory ("bench-top") experiment that exhibits the step-response of a torsional system that contains one or two clearance non-linearities located at different locations (to allow single and dual-clearance cases); 2) Verify the feasibility of the proposed experiment by comparing typical measurements with predictions from simple, low-dimensional non-linear models and 3) Demonstrate the utility of the proposed experiment (denoted X1) through comparative studies between a single-clearance configuration and to a large-scale laboratory experiment (denoted X2 in this paper) [8].

3. Conceptual design considerations

First, it is assumed that clearance non-linearities (with torsional stiffness $k(\theta)$, where θ is the relative angular displacement) can be described by a general piecewise linear form as illustrated in Fig. 1. Here, $\Phi(\theta)$ is the elastic torque transmitted through the clearance, subscripts I and II denote stages (where stage I is the clearance), k_j is the torsional stiffness (linear) of stage j, and Θ_j is the angular transition from stage j to $j+\mathrm{I}$. For the sake of simplicity, the clearance is assumed to be symmetric about $\theta = 0$ and static stiffness values are known (and valid under dynamic conditions) while ignoring contact mechanics. Accordingly, $k(\theta)$ and $\Phi(\theta)$ are defined by the following expressions where sgn is the triple valued sign function and Ξ is the unit-step function:

$$k(\theta) = k_{\mathrm{I}} + (k_{II} - k_{\mathrm{I}})\Xi(|\theta| - \Theta_{\mathrm{I}}), \tag{1}$$

$$\Phi(\theta) = k_{\mathrm{I}}\theta + \mathrm{sgn}(\theta)(k_{\mathrm{II}} - k_{\mathrm{I}})(|\theta| - \Theta_{\mathrm{I}})\Xi(|\theta| - \Theta_{\mathrm{I}}). \tag{2}$$

Next, the proposed experiment (in its dual, single, and no-clearance configurations) is conceptually described by the non-linear models illustrated in Fig. 2. Here, J is the torsional inertia, k is the torsional stiffness (linear), h is the Coulomb friction coefficient, T is the external torque, subscripts $\{A, B, C\}$ are coordinate and element indices, and $\{\theta,\ \dot{\theta},\ \ddot{\theta}\}$ are the angular displacement, velocity, and acceleration, respectively (see Appendix A for a full list of symbols). The dual-clearance configuration (denoted X1-2 and shown in Fig. 2a) is a three degree of freedom (3DOF) positive-definite system that contains two clearance non-linearities ($k_{AB}(\theta_{AB})$ and $k_C(\theta_C)$) and has the following set of governing equations:

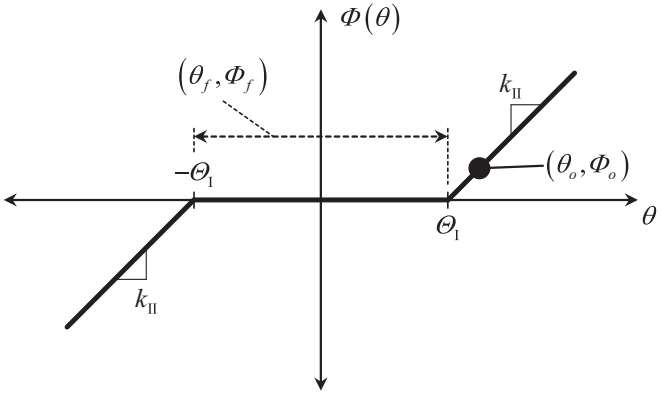

Fig. 1. Illustration of an angular symmetric clearance element $k(\theta)$. Here, elastic torque transmission is given by $\Phi(\theta)$, θ is the relative angular displacement, Θ_I is the angular transition between stage I (clearance with torsional stiffness $k_I = 0$) and II, k_{II} is the torsional stiffness of stage II, (θ_o, Φ_o) is the initial operating point, and (θ_f, Φ_f) is the final operating point.

$$\begin{aligned} J_A\ddot{\theta}_A + h_A \tanh(\eta\dot{\theta}_A) + h_{AB} \tanh(\eta\dot{\theta}_{AB}) + \Phi_{AB}(\theta_{AB}) &= T_A(t), \\ J_B\ddot{\theta}_B - h_{AB} \tanh(\eta\dot{\theta}_{AB}) + h_{BC} \tanh(\eta\dot{\theta}_{BC}) - \Phi_{AB}(\theta_{AB}) + k_{BC}\theta_{BC} &= 0, \\ J_C\ddot{\theta}_C - h_{BC} \tanh(\eta\dot{\theta}_{BC}) + h_C \tanh(\eta\dot{\theta}_C) - k_{BC}\theta_{BC} + \Phi_C(\theta_C) &= 0. \end{aligned} \tag{3a-c}$$

Here, $\Phi_{AB}(\theta_{AB})$ and $\Phi_C(\theta_C)$ are the elastic torque transmissions (as defined by Eq. (2)) through $k_{AB}(\theta_{AB})$ and $k_C(\theta_C)$, respectively. Clearance element $k_{AB}(\theta_{AB})$ (key and keyway) is located between torsional inertias J_A (torsion arm and shaft) and J_B (jaw coupling hub), and $k_C(\theta_C)$ (key and keyway) is located between J_C (jaw coupling hub) and ground. It is assumed that $k_{AB}(\theta_{AB})$ and $k_C(\theta_C)$ are identical, and thus share the same values of Θ_j and k_j. A torsional spring (linear) k_{BC} (achieved via coil springs between the coupling jaws) is utilized to couple J_B to J_C. Similar to prior work [8] concerning clutch dampers, it is assumed that all dissipative elements (which include: h_A (shaft and bearing interface), h_{AB} (shaft and coupling hub interface), h_{BC} (coil springs), and h_C (shaft and coupling hub interface)) can be simply described by a Coulomb friction model (hyperbolic tangent approximation where η is a regularizing factor [12]). The hyperbolic tangent approximation is chosen (instead of the signum function) to reduce the computational time for numerical solving algorithms. Lastly, system excitation is provided by an external torque $T_A(t)$ that is applied to inertia J_A ($T_B = T_C = 0$); $T_A(t)$ is a step-down at time $t = 0$ from initial T_{Ao} to final T_{Af} torque values and is defined by the following:

$$T_A(t) = T_{Ao}\left[1 - \Xi(t)\right] + T_{Af}\Xi(t). \tag{4}$$

The single-clearance configuration (denoted X1-1a and shown in Fig. 2b) is a two degree of freedom (2DOF) positive-definite system that contains one clearance element ($k_{AB}(\theta_{AB})$) Here, $k_C(\theta_C) \to \infty$ such that J_C is fixed to ground. There is an alternate version (say X1-1b) in which $k_C(\theta_C)$ is the sole clearance element (J_C is free to vibrate but $k_{AB}(\theta_{AB}) \to \infty$). However, version X1-1a is favored over X1-1b for two reasons: i) Element $k_{AB}(\theta_{AB})$ is closer to the excitation $T_A(t)$, thus it influences the step-response more that $k_C(\theta_C)$; and ii) The layout of X1-1a is analogous to a prior large-scale experiment [8] such that $k_{AB}(\theta_{AB})$ is similar to a spline clearance (or a very compliant spring) and k_{BC} may be considered a linearized clutch damper. The single-clearance configuration (X1-1a) is a simplified case of X1-2; hence, X1-1a has the following set of governing equations, which are derived from Eq. (3):

$$\begin{aligned} J_A\ddot{\theta}_A + h_A \tanh(\eta\dot{\theta}_A) + h_{AB} \tanh(\eta\dot{\theta}_{AB}) + \Phi_{AB}(\theta_{AB}) &= T_A(t), \\ J_B\ddot{\theta}_B - h_{AB} \tanh(\eta\dot{\theta}_{AB}) + h_{BC} \tanh(\eta\dot{\theta}_{BC}) - \Phi_{AB}(\theta_{AB}) + k_{BC}\theta_B &= 0. \end{aligned} \tag{5a-b}$$

Lastly, the no-clearance configuration (denoted X1-0 and shown in Fig. 2c) is a single degree of freedom (1DOF) positive-definite, linear time-invariant system as both clearance elements are removed ($k_{AB}(\theta_{AB}) \to \infty$ and $k_C(\theta_C) \to \infty$) so that J_A is rigidly attached to $J_B(\theta_A = \theta_B)$ and J_C is fixed to ground. Similar to X1-1a, configuration X1-0 is a simplification of X1-2; accordingly, its (X1-0) governing equation is the following:

$$(J_A + J_B)\ddot{\theta}_A + h_A \tanh(\eta\dot{\theta}_A) + h_{BC} \tanh(\eta\dot{\theta}_{BC}) + k_{BC}\theta_A = T_A(t). \tag{6}$$

This configuration (X1-0) serves several important roles as it provides much needed no-impact benchmark data for comparison while representing a special constant-contact case (where $|\theta_{AB}| > \Theta_{AB\_I}$) of the single-clearance configuration (X1-1a). Crucial system parameters (including J_A and h_A) can be estimated from its step-response.

The following experimental design objectives are identified to ensure the relevance and applicability to the literature [4–8]:

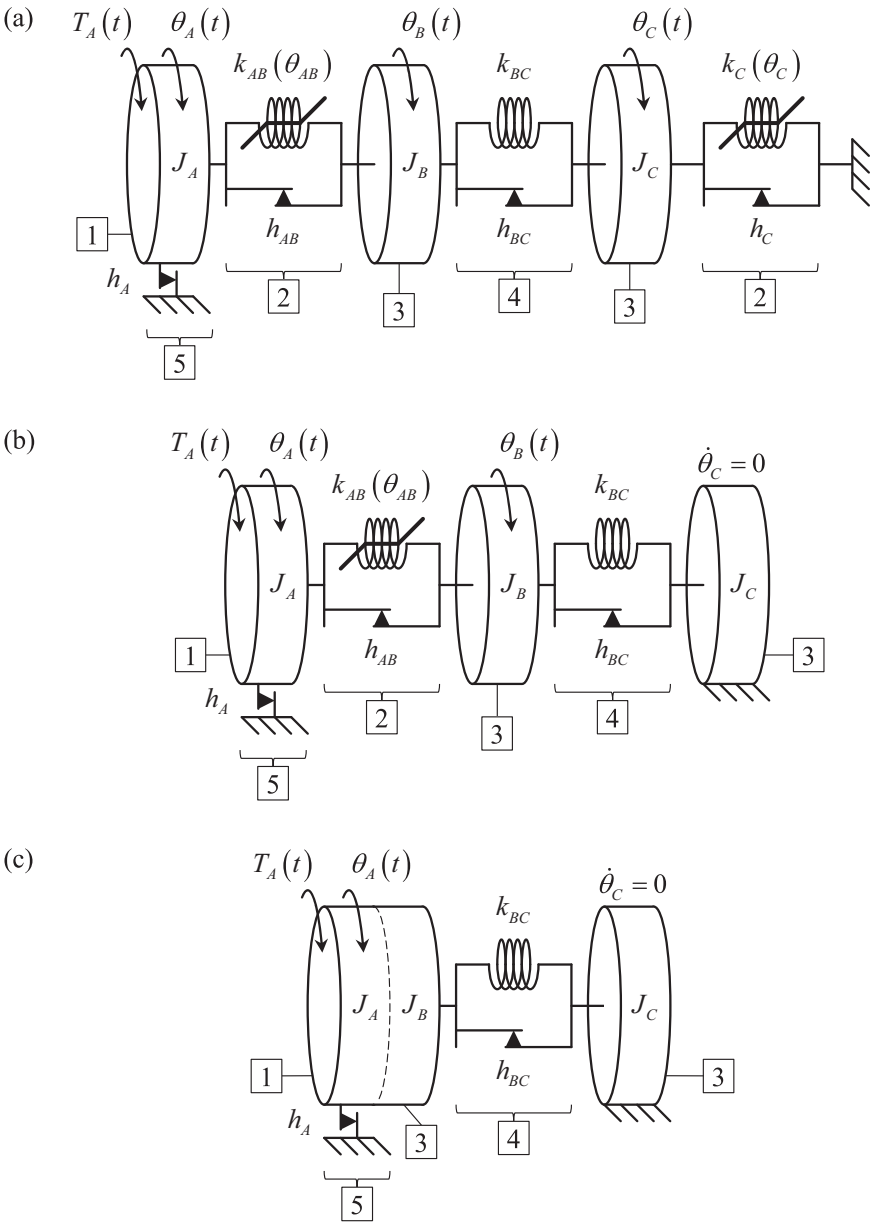

Fig. 2. Conceptual illustration of the proposed experiment X1 with clearances as defined in Fig. 1: a) dual-clearance configuration (X1-2); b) single-clearance configuration (X1-1a); and c) no-clearance configuration (X1-0). Here, $\{\theta, \dot{\theta}\}$ is the angular displacement and velocity (respectively), J is the torsional inertia, k is the torsional stiffness, h is the Coulomb friction, and T is the external torque. Subscripts $\{A, B, C\}$ are element and coordinate indices. Key: 1 – torsion arm, shaft, and disks; 2 – key and keyway (clearance); 3 – coupling hub; 4 – torsional spring (linear); and 5 – shaft and bearing interface.

1. The experiment must qualify as "bench-top," meaning its footprint must fit on a typical table-top found in a laboratory setting (say approximately 1 m by 0.5 m);
2. For sizing purposes, the first torsional mode of all configurations must have a natural frequency (ω_{n_1}) between 5 and 15 Hz (with a corresponding natural period τ_{n_1} between 0.07 and 0.2 s), similar to a vehicle driveline and prior experiments [4–8];
3. The first flexural mode of the torsion arm within the plane of rotation must have a frequency greater than $10\omega_{n\_1}$ to avoid interference with the dynamics of interest;
4. Coulomb friction must be minimized so that non-linear behavior is controlled by the clearance elements;
5. To ensure vibro-impact phenomena, the initial ($(\theta_{AB\_o}, \Phi_{AB\_o})$ and (θ_{Co}, Φ_{Co})) and final ($(\theta_{AB\_f}, \Phi_{AB\_f})$ and $(\theta_{C\_o}, \Phi_{C\_o})$) operating points at the clearances must lie on separate stages (see Fig. 1); and
6. The experiment must be instrumented to measure time domain angular acceleration signals, which is consistent with prior work [4–8].

4. Physical design, instrumentation, and measurement considerations

The proposed experiment is physically illustrated (for the sake of clarity) by the simplified solid model shown in Fig. 3. First, a steel baseplate that has a footprint of approximately 50 cm^2 and can be bolted or clamped onto a laboratory work surface is selected. Next, a sleeve bearing is chosen and bolted to the baseplate; a corresponding keyed shaft (of length L_{shaft}, radius R_{shaft}, and material density ρ_{shaft}) is supported by the bearing. A torsion arm (of length L_{arm_x}, height L_{arm_y}, thickness L_{arm_z}, and material density ρ_{arm}) is then rigidly attached to the shaft. Steel disks (with radius R_{disk}, thickness L_{disk_z}, and material density ρ_{disk}) are then adhered to bottom-side of the torsion arm at both of its ends; a symmetrical layout is chosen so that the final operating point has a near zero torque ($T_{Af} \approx 0$). These components compose J_A as defined by $J_A = J_{shaft} + J_{arm} + 2J_{disk}$ where J_{shaft}, J_{arm}, and J_{disk} are the torsional inertias of the shaft, torsion arm, and a single disk, respectively, and are approximated by the following [13]:

$$J_{shaft} \approx 0.5\pi\rho_{shaft}R_{shaft}L_{shaft}^4, \tag{7}$$

$$J_{arm} \approx \rho_{arm}L_{arm\_x}L_{arm\_y}L_{arm\_z}\left(L_{arm\_x}^2 + L_{arm\_y}^2\right)/12, \tag{8}$$

$$J_{disk} \approx \pi\rho_{disk}L_{disk\_z}R_{disk}^2\left[\left(3R_{disk}^2 + L_{disk\_z}^2\right)/12 + \left(L_{arm\_x} - R_{disk}\right)^2\right]. \tag{9}$$

Next, a jaw coupling set, consisting of an elastomer spider and two identical hubs with keyways and set screws (see [14] for an example), is chosen. One of the hubs (J_B) mates to the keyed shaft on the end opposite to the torsion arm; the other hub (J_C) mates to a separate short keyed shaft that is fixed to the baseplate. The key and keyway interfaces between the hubs and shafts provide clearance elements $k_{AB}(\theta_{AB})$ and $k_C(\theta_C)$. The clearance gaps (Θ_{AB} and Θ_C) are controlled by the key widths. It should be noted that various gaps and stiffness values can be achieved by altering the dimensions and material of the key. If the set screw is tightened at either location, the hub becomes rigidly attached to the shaft (i.e. $k_{AB}(\theta_{AB}) \to \infty$ and $k_C(\theta_C) \to \infty$). The elastomer spider between the hubs is removed and replaced by six coil springs, each with translational stiffness k_{spring} (measured under static loading). Accordingly, torsional stiffness k_{BC} is defined by the expression $k_{BC} = 6k_{spring}R_{spring}^2$ where R_{spring} is the radial distance to the centerline of the coil springs:

It is assumed that the first torsional mode of all experiment configurations can be approximated by the natural frequency of configuration X1-0, as defined by:

$$\omega_{n\_1} = \left[k_{BC}/\left(J_A + J_B\right)\right]^{0.5}. \tag{10}$$

Because the coil springs and coupling hubs are purchased components, it is easier to control ω_{n_1} through J_A. For the sake of convenience, torsion arm length L_{arm_x} is selected so that 5Hz $\leq \omega_{n\_1} \leq$ 15Hz. However, L_{arm_x} must also be chosen so that the frequency of the first flexural mode of the torsion arm within the plane of rotation (say ω_{arm_1}) is greater than $10\omega_{n\_1}$. This is verified by approximating the torsion arm as a cantilevered beam of length $L'_{arm\_x} = 0.5L_{arm\_x} - 2R_{disk}$ with a point mass $m' = \pi\rho_{disk}R_{disk}^2L_{disk\_z} + 2\rho_{arm}R_{disk}L_{arm\_y}L_{arm\_z}$ at its end [15]. The characteristic equation of this beam is defined by the following where subscript r is the modal index, β_r is the rth wave number ($\beta_r = (\omega_{arm\_r}^2\gamma_{arm}E_{arm}^{-1}I_{arm}^{-1})^{0.25}$), γ_{arm} is the mass per unit length of the torsion arm ($\gamma_{arm} = \rho_{arm}L_{arm\_y}L_{arm\_z}$), E_{arm} is the Young's modulus of the arm material, and I_{arm} is the area moment of inertia of the arm's cross section ($I_{arm} = L_{arm\_y}^3L_{arm\_z}/12$) [13,15]:

$$\frac{\beta_r^3\left\{2\gamma_{arm}\left[1 + \cos\left(\beta_rL'_{arm\_x}\right)\cosh\left(\beta_rL'_{arm\_x}\right)\right] + \ldots \right.}{\left. \frac{2m'\beta_r\left[\cos\left(\beta_rL'_{arm\_x}\right)\sinh\left(\beta_rL'_{arm\_x}\right) - \cosh\left(\beta_rL'_{arm\_x}\right)\sin\left(\beta_rL'_{arm\_x}\right)\right]}{\gamma_{arm}\left[\cos\left(\beta_rL'_{arm\_x}\right) + \cosh\left(\beta_rL'_{arm\_x}\right)\right]}\right\} = 0.} \tag{11}$$

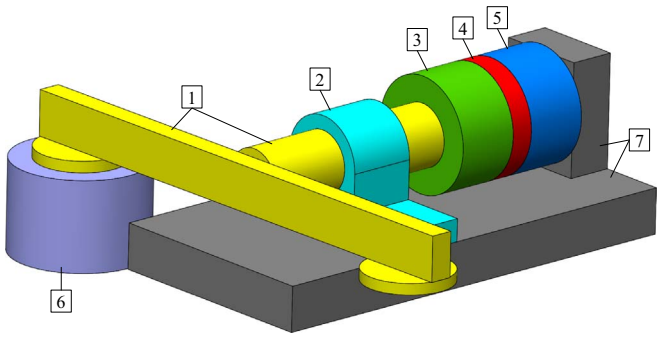

Fig. 3. Solid model of the proposed experiment X1 as conceptually described in Fig. 2. Key: 1 – torsion arm, shaft, and disks (J_A); 2 – bearing; 3 – coupling hub (J_B); 4 – coil spring sets between coupling jaws; 5 – coupling hub (J_C); 6 – electromagnet mass drop; and 7 – base plate.

Next, Eq. (11) is solved (numerically) for the smallest positive value of β_r, yielding β_1 and subsequently $\omega_{\text{arm\_1}} = (\beta_1^4 E_{\text{arm}} I_{\text{arm}} \gamma_{\text{arm}}^{-1})^{0.5}$.

After the experiment is assembled, the torsional inertias are estimated using solid modeling software [16] (where ρ is estimated from the measured mass and volume of the respective physical component) and the flexural mode of the torsion arm is verified using commercial finite element code [17]. Additionally, k_{BC} is estimated by applying known torque values (with finite increments of ΔT_A) to the torsion arm (in configuration X1-0) and measuring the resulting relative displacement $\Delta\theta_A$ with a digital level to the nearest 0.1° [18] (see Appendix B for a list of hardware and instrumentation). The system natural frequency ω_{n_1} is then checked by substituting the estimated values of J_A, J_B, and k_{BC} into Eq. (10).

Next, it is necessary to reduce the effect of dissipative elements (e.g. dry friction) and thus, the experiment is assembled so that shaft, bearing, and coupling hubs are well aligned (this reduces the normal forces at radial interfaces). Additionally, Teflon sheeting is adhered to sliding interfaces (where possible), such as between the coupling hubs.

Finally, an electromagnet mass drop is chosen to provide the external torque $T_A(t)$, similar to prior work [5–7]. For time $t < 0$, the electromagnet (with additional mass) is attached to one of the steel disks on the torsion arm, as shown in Fig. 3. At $t = 0$, a switch disrupts the electrical current and the electromagnet (with additional mass) falls away from the disk. The amount of additional mass is determined by the torque required to fully displace spring k_{BC} (say by $\theta_{BC\_\max}$, thus $T_{Ao} = k_{BC}\theta_{BC\_\max}$). This ensures that the initial operating point at each clearance is within stage II (i.e. contact), and maximizes the initial energy of the system.

To measure the angular motions, a translational accelerometer [19] (see Appendix B for specifications) is attached to each torsional inertia at a radial distance R_j, as shown in Fig. 4. The measured translational acceleration signals $\ddot{q}_j$ are recorded by a commercial data acquisition system [20,21] and computer with associated software [22]. Measurement is triggered by a threshold value of $\ddot{q}_A$, which is judiciously chosen so that the step consistently occurs near $t = 0$ for all configurations. Sampling frequencies of 12.8, 25.6, and 51.2 kHz are initially considered, and it is found that peak to peak values of $\ddot{\theta}_A(t)$ (for the single (X1-1a) and dual-clearance (X1-2) configurations) increase with sampling frequency. Although this is a significant observation, a sampling frequency of 12.8 kHz is chosen because the truly impulsive nature of the response is not a primary concern of this study. Next, it is assumed that measured signals $\ddot{q}_j$ are tangential to the corresponding angular motions, thus angular accelerations $\ddot{\theta}_j$ are calculated using the following equation:

$$\ddot{\theta}_j = \ddot{q}_j R_j^{-1}, \quad j = A, B, C \tag{12}$$

Typical measured angular accelerations (normalized) for the no (X1-0), single (X1-1a), and dual-clearance (X1-2) configurations are shown in Figs. 5–7, respectively; the typical external torque $T_A(t)$ (all configurations) is shown in Fig. 5b. Here, time is scaled by $\tau_{n\_1} = 2\pi/\omega_{n\_1}$, angular acceleration by $\theta_{AB\_\max}\tau_{n\_1}^{-2}$, and torque by $k_{BC}\theta_{BC\_\max}$. Several important observations are made. First, the measured motion of the no-clearance configuration (X1-0) appears to be almost linear and its oscillatory period $\bar{\tau}_{\text{osc}}$ (defined by the elapsed time between extrema and then normalized) is nearly constant. Additionally, the nature of the amplitude decay is neither distinctly linear nor exponential. In contrast, the measured motions of the single (X1-1a) and dual-clearance (X1-2) configurations clearly exhibit rich non-linear behavior. In both X1-1a and X1-2, the double-sided impact regime (denoted di) is observed across the entire response (with amplitudes about 20 times greater than in X1-0). Prior work [8] has shown that these impacts occur when there is a sudden change from a relatively low (or zero) to high stiffness level, such as from k_{j_I} to k_{j_II} at $\pm\Theta_{j\_\text{I}}$. It is also noted that $\bar{\tau}_{\text{osc}}$ increases (nearly exponentially) by about 40% from the first to last oscillatory period (softening effect). Furthermore, the response durations of the clearance

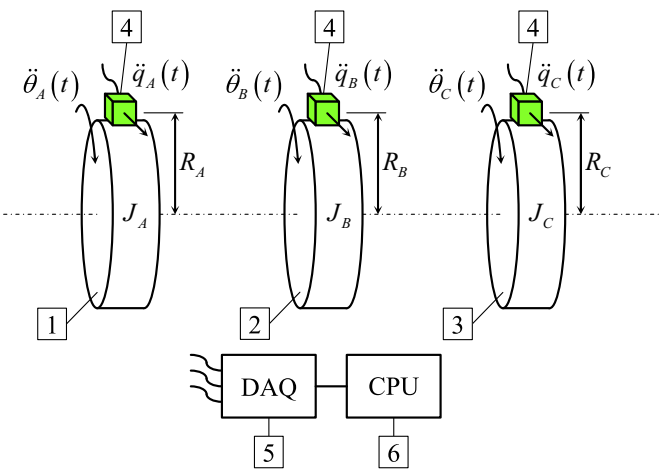

Fig. 4. Instrumentation schematic for experiment X1. Here, $\ddot{\theta}$ is the calculated angular acceleration, $\ddot{q}$ is the measured translational acceleration, J is the torsional inertia, and R is the radial distance from the axis of rotation to the translational accelerometers [19]. Key: 1 – torsion arm, shaft, and disks; 2 – coupling hub; 3 – coupling hub; 4 – translational accelerometer; 5 – data acquisition device (DAQ) [20,21]; and 6 – computer (CPU) [22].

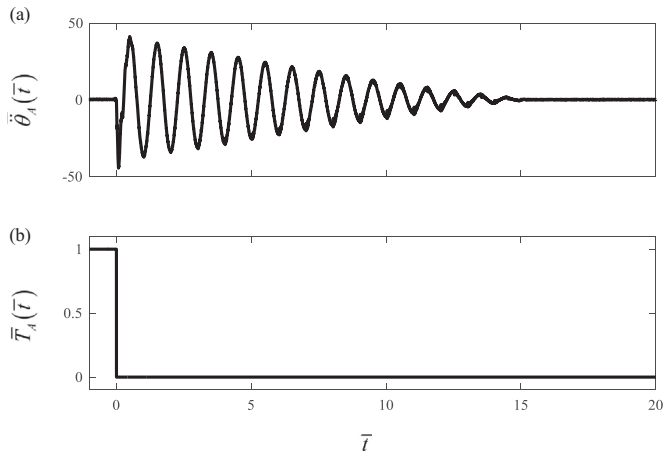

Fig. 5. Measured (normalized) angular acceleration a) $\ddot{\bar{\theta}}_A(\bar{t})$ for the no-clearance configuration of Fig. 2c (X1-0), given b) step-like excitation $\bar{T}_A(\bar{t})$.

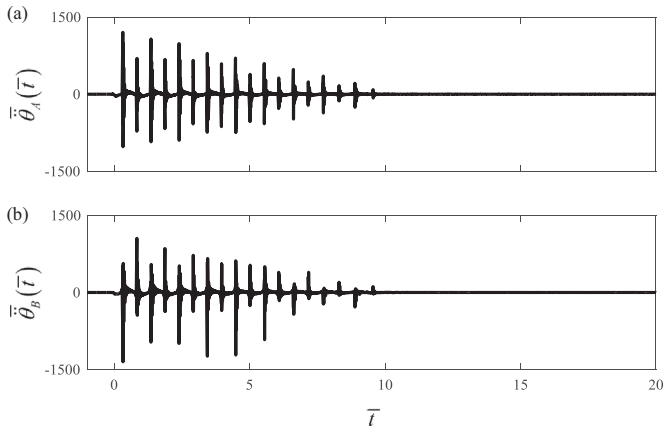

Fig. 6. Measured angular accelerations for the single-clearance configuration of Fig. 2b (X1-1), given step-like excitation $\bar{T}_A(\bar{t})$ of Fig. 5b: a) $\ddot{\bar{\theta}}_A(\bar{t})$; and b) $\ddot{\bar{\theta}}_B(\bar{t})$.

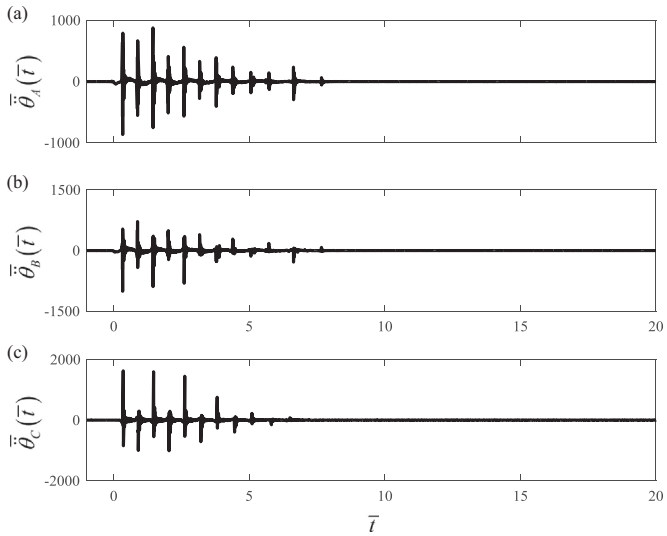

Fig. 7. Measured angular accelerations for the dual-clearance configuration of Fig. 2a (X1-2), given step-like excitation $\bar{T}_A(\bar{t})$ of Fig. 5b: a) $\ddot{\bar{\theta}}_A(\bar{t})$; b) $\ddot{\bar{\theta}}_B(\bar{t})$; and c) $\ddot{\bar{\theta}}_C(\bar{t})$.

configurations (X1-1a and X1-2) are much shorter than that of the no-clearance configuration (X1-0). This suggests that there are additional dissipative elements in X1-1a and X1-2, such as the sliding interfaces h_{AB} and h_C, and possibly impact damping (though this issue is beyond the scope of the paper). In the next section, the proposed experiment will be verified by comparing measurements to predictions from the non-linear models shown in Fig. 2.

5. Verification of the experiment via comparison with non-linear model(s)

Since all linear and non-linear model parameters must be estimated prior to the simulation, necessary parameters, methods, and their procedural sequence are listed in Table 1. First, k_{BC} is estimated (as stated in Section 4) by applying known static torque values (with relative amplitudes ΔT_A) to the J_A element (in the no-clearance configuration X1-0) and measuring the resulting change in angular displacement $\Delta\theta_A$ with a digital level [18]; accordingly, $k_{BC} = \Delta T_A/\Delta\theta_A$. Next, a sub-experiment (denoted X1-P1 and conceptually illustrated in Fig. 8a) is proposed to estimate torsional inertia J_B and Coulomb friction h_{BC}. It is built by removing J_A from the single-clearance configuration (X1-1a) and has the following governing equation where $T_B(t)$ is an impulsive external torque applied to J_B via an impulse hammer:

$$J_B\ddot{\theta}_B + h_{BC}\tanh\left(\eta\dot{\theta}_B\right) + k_{BC}\theta_B = T_B(t). \tag{13}$$

The angular acceleration $\ddot{\theta}_B(t)$ is calculated from the measured translational acceleration $\ddot{q}_B(t)$, as shown in Fig. 4 and given by Eq. (12). The value of J_B (which includes the translational accelerometer) is then extracted from $J_B = k_{BC}(\tau_{\mathrm{osc}\_\mu}/2\pi)^2$ where τ_{osc_μ} is the average oscillatory period of the measured response $\ddot{\theta}_B(t)$. Due to similarity, it is assumed that $J_C = J_B$. The value of h_{BC} is estimated from the near-linear decay of the amplitude [15].

Next, the step-response (shown in Fig. 5a) of the no-clearance configuration (X1-0) is utilized to estimate J_A (including a translational accelerometer) and h_A. Like the sub-experiment X1-P1, J_A is estimated from $J_A = k_{BC}(\tau_{\mathrm{osc}\_\mu}/2\pi)^2 - J_B$ where τ_{osc_μ} is the average oscillatory period of the step-response (Fig. 5a). It is assumed that the response amplitude decay is nearly linear and that the total Coulomb friction amplitude $h_A + h_{BC}$ can be estimated as before [15]; as h_{BC} is already known, h_A is easily calculated. A second sub-experiment (denoted X1-P2 and shown in Fig. 8b) is proposed to estimate Coulomb friction h_{AB}. It is a modified version of the single-clearance experiment (X1-1a), where $k_{AB}(\theta_{AB}) = 0$ and J_B is fixed to the ground, and thus given by the following:

$$J_A\ddot{\theta}_A + (h_A + h_{AB})\tanh\left(\eta\dot{\theta}_A\right) = T_A(t). \tag{14}$$

The external torque $T_A(t)$ is applied to the J_A element via a translational spring scale at the end torsion arm. Here, $T_A(t)$ is slowly increased from zero amplitude (at $t = 0$) until sliding (at constant velocity) occurs, and then it is slowly decreased until sticking occurs (say at $T_A(t) = T_{\mathrm{stick}}$). It is assumed that $h_{AB} \approx T_{\mathrm{stick}} - h_A$.

A third sub-experiment (denoted X1-P3 shown in Fig. 8c) is proposed for the estimation of Θ_{AB_I} and k_{AB_II}. It is constructed by removing all components except J_C, $k_C(\theta_C)$, and h_C from the dual-clearance configuration (X1-2) and it is given by the following:

$$J_C\ddot{\theta}_C + h_C\tanh\left(\eta\dot{\theta}_C\right) + \Phi_C(\theta_C) = T_C(t). \tag{15}$$

Here, $T_C(t)$ is applied to the J_C element via a torsion arm with variable mass at its end (the subsequent measurements occur under static conditions, thus the additional torsional inertia of the arm and mass is inconsequential). The angular displacement θ_C is calculated to the nearest 0.01° using $\theta_C = q_C R_{\mathrm{probe}}^{-1}$ where q_C is the translational displacement measured by a probe [23] located at radial distance R_{probe} (where it is assumed that q_C is tangential to θ_C). First, J_C is moved between the two contact points of the clearance $k_C(\theta_C)$ and the relative angular displacement (say θ_{gap}) is measured. It has been assumed that the clearance elements are symmetric, thus $\Theta_{C\_\mathrm{I}} = 0.5\theta_{\mathrm{gap}}$. Torsional inertia J_C is then positioned at either $\pm\Theta_{C\_\mathrm{I}}$ and known static torque values (with relative amplitudes ΔT_C) are applied to J_C via a torsion arm and variable masses. The

Table 1
Summary of the necessary system parameters (including the sequence, method of estimation, and corresponding figure) for non-linear models of the proposed experiment (X1).

Sequence of estimation	Estimated parameter(s)	Method and corresponding figure
1st	k_{BC}	No-clearance configuration X1-0 (static loading) – Fig. 2c
2nd	J_B, J_C, and h_{BC}	Sub-experiment X1-P1 – Fig. 8a
3rd	J_A and h_A	No-clearance configuration X1-0 (step-response) – Fig. 2c
4th	h_{AB} and h_C	Sub-experiment X1-P2 – Fig. 8b
5th	Θ_{AB_I}, Θ_{C_I}, k_{AB_II}, and k_{C_II}	Sub-experiment X1-P3 – Fig. 8c

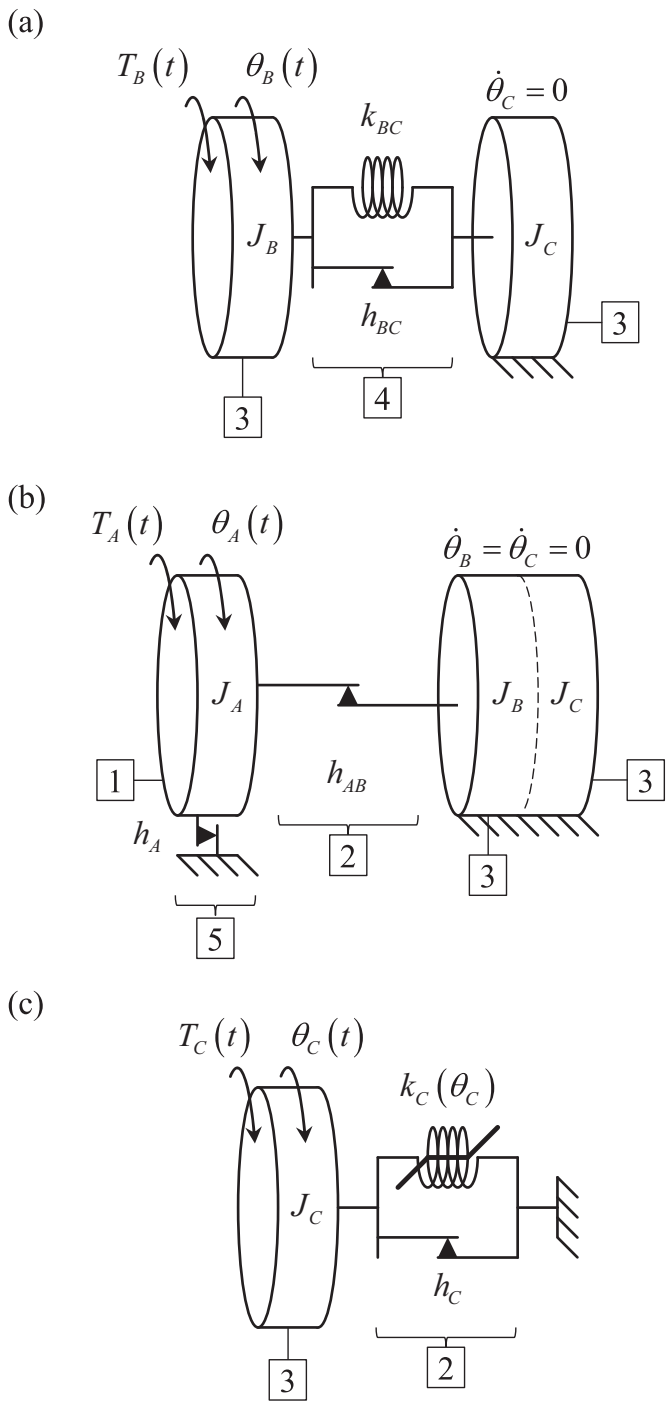

Fig. 8. Sub-experiments of X1 utilized for parameter estimation: a) sub-experiment X1-P1 (estimation J_B and h_{BC}); b) sub-experiment X1-P2 (estimation h_{AB}); and c) sub-experiment X1-P3 (estimation of Θ_{AB_I} and k_{AB_II}). Here, $\{\theta, \dot{\theta}\}$ is the angular displacement and velocity (respectively), J is the torsional inertia, k is the torsional stiffness, h is the Coulomb friction, and T is the external torque. Subscripts $\{A, B, C\}$ are element and coordinate indices. Key: 1 – torsion arm, shaft, and disks; 2 – key and keyway (clearance); 3 – coupling hub; 4 – torsional spring (linear); and 5 – shaft and bearing interface.

resulting change in angular displacement $\Delta\theta_C$ is measured and stiffness k_{C_II} is calculated using $k_{C\_II} = \Delta T_C/\Delta\theta_C$. Nevertheless, measurements reveal that k_{C_II} is very stiff compared to k_{BC} (say by a factor of nearly 200); thus, the value of k_{C_II} is approximated as $k_{C\_II} \approx 200k_{BC}$. Recall from Section 3, it is assumed that $k_{AB\_II} = k_{C\_II}$ and $\Theta_{AB\_I} = \Theta_{C\_I}$.

After the parameter estimation process is complete, the step-responses of each configuration are predicted by numerically integrating the corresponding governing equations (Eq. (3) for X1-2, Eq. (5) for X1-1a, and Eq. (6) for X1-0).

Several variable order and time-step Runge-Kutta algorithms [24] are used and the maximum allowable time-step and resolution of the resulting time array are set equal to the sampling period of the measurements (about 78.1 μs). Since there is negligible difference between the integration algorithms, the non-linear simulation is considered successful. First, a comparison between the measurement and prediction for the no-clearance configuration (X1-0) is shown in Fig. 9. The motions have nearly equivalent oscillatory periods (in terms of duration and quantity) along with peak to peak acceleration amplitudes, which are listed in Table 2. This agreement provides fidelity to the parameter estimation process as well as the instrumentation and signal processing method employed. Next, measured and predicted motions of the single-clearance configuration (X1-1a) are compared in Fig. 10. Additionally, peak to peak values and times of occurrence for selected impacts (which are labeled in Fig. 10) are listed in Tables 3 and 4, respectively. Both predicted and measured motions exhibit the double-sided impact regime and have very similar duration (about 18 impacts and 9 or 10 oscillatory periods). However, the predicted motions seem to have a lead that increases with time as clearly observed in the times of occurrence in Table 4. Although the reduced-order non-linear model fails to predict the precise peak to peak values of impacts in $\bar{\ddot{\theta}}_A(\bar{t})$, it is relatively accurate with respect to the impacts in $\bar{\ddot{\theta}}_B(\bar{t})$ (say within a factor of 2) and long time-scale motions (which are nearly sinusoidal with an oscillatory period of about $\bar{\tau}_{n\_1}$ in both $\bar{\ddot{\theta}}_A(\bar{t})$ and $\bar{\ddot{\theta}}_B(\bar{t})$).

Finally, a comparison between the measurement and prediction for the dual-clearance configuration (X1-2) is shown in Fig. 11 and their peak to peak values as well as times of occurrence for impacts (as labeled in Fig. 11) are shown in Tables 5 and 6, respectively. Most comments regarding the predictions of X1-1a also apply to X1-2 except for two notable differences. First, the prediction (X1-2) exhibits one more oscillatory period (and about two more impacts) than the measurement for some responses, and secondly, the leading effect of the prediction is much greater in X1-2 than seen previously in X1-1a. Overall, the predicted and measured motions (for all configurations) exhibit similar quantitative (in some aspects) and qualitative behavior, which verifies the feasibility of the experiment. To improve the accuracy of the predictions, refined higher-dimensional non-linear models must be considered.

6. Relevance and applicability to a large-scale experiment

As stated in Section 3, the single-clearance configuration (X1-1a) is analogous to the large-scale experiment recently proposed by Krak et al. [8] (denoted X2). The prior experiment [8] can be simply described by a 1DOF non-linear model with torsional inertia J, multi-staged torsional stiffness element $k(\theta)$, multi-staged dry friction element $h(\theta)$, step-like external torque $T(t)$, and angular displacement, velocity, and acceleration $\{\theta, \dot{\theta}, \ddot{\theta}\}$, respectively (see [8] for a schematic and full discussion). In particular, the stiffness $k(\theta)$ and dry friction $h(\theta)$ elements are provided by a production vehicle clutch damper. The elastic torque transmission $\Phi(\theta)$ for two example cases (denoted C1 [8] and C2) is illustrated in Fig. 12. Both C1 and C2 contain four-stages; stages II–IV are a pre-load feature, main operating stage, and stopper, respectively. Stage I has a

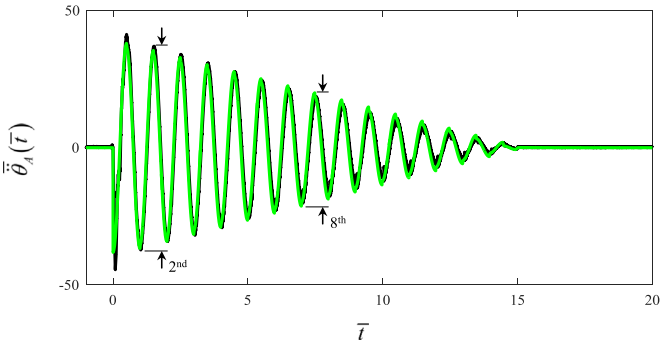

Fig. 9. Measured and predicted angular acceleration $\bar{\ddot{\theta}}_A(\bar{t})$ (normalized) step-response of the no-clearance configuration (X1-0). Key: (▬) – measurement; and (▬) – prediction. Here, (*j*th) marks are the peak to peak values of their oscillatory periods.

Table 2
Measured and predicted peak to peak values for oscillatory periods in $\bar{\ddot{\theta}}_A(\bar{t})$ of the no-clearance configuration (X1-0) given step excitation.

	Peak to peak value (normalized) for oscillatory period number						
	2nd	4th	6th	8th	10th	12th	14th
Measurement	74	63	50	38	26	17	8.3
Prediction	72	62	52	41	31	21	10

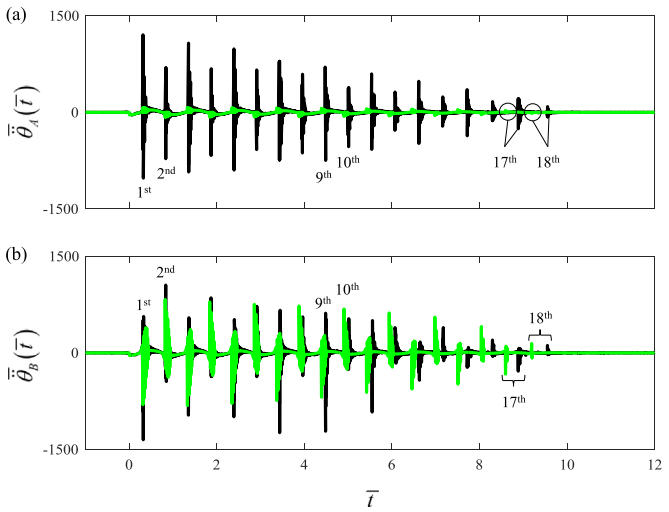

Fig. 10. Measured and predicted angular accelerations $\ddot{\bar{\theta}}_A(\bar{t})$ and $\ddot{\bar{\theta}}_B(\bar{t})$ (normalized) step-response of the single-clearance configuration (X1-1a). Key: (▬) – measurement; and (▬) – prediction. Here, (jth) impacts are marked.

Table 3
Measured and predicted peak to peak values for selected impacts: a) in $\ddot{\bar{\theta}}_A(\bar{t})$ and b) in $\ddot{\bar{\theta}}_B(\bar{t})$ of the single-clearance configuration (X1-1a) given step excitation.

	Peak to peak value (normalized) for impact number					
	1st	2nd	9th	10th	17th	18th
a) $\ddot{\bar{\theta}}_A(\bar{t})$						
Measurement	2230	1420	1450	920	470	160
Prediction	78	80	66	65	33	18
b) $\ddot{\bar{\theta}}_B(\bar{t})$						
Measurement	1910	1500	1830	790	350	140
Prediction	1200	1210	960	940	430	230

Table 4
Measured and predicted times of occurrence selected impacts: a) in $\ddot{\bar{\theta}}_A(\bar{t})$ and b) in $\ddot{\bar{\theta}}_B(\bar{t})$ of the single-clearance configuration (X1-1a) given step excitation.

	Time of occurrence (normalized) for impact number					
	1st	2nd	9th	10th	17th	18th
a) $\ddot{\bar{\theta}}_A(\bar{t})$						
Measurement	0.31	0.83	4.47	5.01	8.88	9.56
Prediction	0.31	0.82	4.39	4.91	8.59	9.19
b) $\ddot{\bar{\theta}}_B(\bar{t})$						
Measurement	0.32	0.83	4.48	5.01	8.88	9.55
Prediction	0.31	0.82	4.39	4.91	8.59	9.19

very compliant spring ($k_l \approx 0$) in C1 and a spline backlash ($k_l = 0$) in C2. The abrupt change in stiffness from stages I to II (in C1 and C2) is similar to the clearance non-linearity contained in the proposed experiment (X1-1a).

The measured angular accelerations $\ddot{\bar{\theta}}(\bar{t})$ for X2-C1 [8] and X2-C2, given a step-like external torque $T(t)$ excitation (with initial and final operating points as labeled in Fig. 12), are shown in Figs. 13a and 14a, respectively. Here, results are normalized where the time is scaled by τ_{n_III} (natural period of stage III) and the angular acceleration is scaled by $\Theta_{IV}/\tau_{n\_III}^2$. The

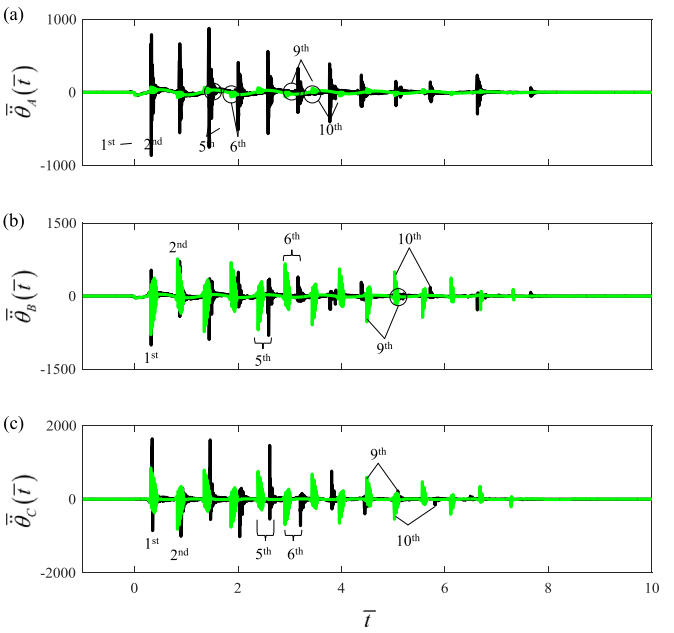

Fig. 11. Measured and predicted angular accelerations (normalized) for step-response of the dual-clearance configuration (X1-2): a) $\ddot{\bar{\theta}}_A(\bar{t})$, b) $\ddot{\bar{\theta}}_B(\bar{t})$, and c) $\ddot{\bar{\theta}}_C(\bar{t})$. Key: (▬) – measurement; and (▬) – prediction. Here, (jth) impacts are marked.

Table 5
Measured and predicted peak to peak values for selected impacts: a) in $\ddot{\bar{\theta}}_A(\bar{t})$, b) in $\ddot{\bar{\theta}}_B(\bar{t})$, c) in $\ddot{\bar{\theta}}_C(\bar{t})$ of the dual-clearance configuration (X1-2) given step excitation.

	Peak to peak value (normalized) for impact number					
	1st	2nd	5th	6th	9th	10th
a) $\ddot{\bar{\theta}}_A(\bar{t})$						
Measurement	1660	1220	1130	610	340	270
Prediction	80	70	70	60	50	50
b) $\ddot{\bar{\theta}}_B(\bar{t})$						
Measurement	1540	1140	1160	506	170	210
Prediction	1170	1120	1000	950	720	670
c) $\ddot{\bar{\theta}}_C(\bar{t})$						
Measurement	2500	1310	2000	880	350	190
Prediction	1220	1170	1050	970	780	700

step-response of both X2-C1 and X2-C2 exhibit double (di), single (si), and no-impact (ni, though not shown for X2-C1 in Fig. 13a) regimes [8,9]. The time of transition between these regimes are denoted by $\bar{t}_{\text{di}}$ (from di to si regimes) and $\bar{t}_{\text{si}}$ (from si to ni regimes). These regimes correspond to travel across stage transitions Θ_{I} and $-\Theta_{\text{I}}$ as discussed in [8]. The responses can be further characterized by the time-varying oscillatory period $\bar{\tau}_{\text{osc}}^{(j)}$, which is defined here as the elapsed (normalized) time between the jth and $(j+1)$th impact at Θ_{I} with a corresponding time of occurrence $\bar{t}_{\text{osc}}^{(j)}$ (median time between the jth and $(j+1)$th impact at Θ_{I}). Points $(\bar{t}_{\text{osc}}^{(j)}, \bar{\tau}_{\text{osc}}^{(j)})$ are labeled in Figs. 13 and 14a and shown in Figs. 13 and 14b (for the di and si regimes only). Observe that points $(\bar{t}_{\text{osc}}^{(j)}, \bar{\tau}_{\text{osc}}^{(j)})$ exhibit asymptotic trends within each regime; for instance, the double-sided impact regime (di) shows a softening effect $(\bar{\tau}_{\text{osc}}^{(j)} \to \infty)$ while the single-sided impact regime (si) has a hardening effect $(\bar{\tau}_{\text{osc}}^{(j)} \to 0)$. This behavior is also exhibited by the single-clearance configuration of the proposed experiment (X1-1a); points $(\bar{t}_{\text{osc}}^{(j)}, \bar{\tau}_{\text{osc}}^{(j)})$ from motion $\ddot{\bar{\theta}}_B(\bar{t})$ are labeled in Fig. 15a and shown in Fig. 15b. Here, only the hardening effect is apparent because the entire response is in the double-sided impact regime (di) only. This qualitative agreement clearly demonstrates the relevance and applicability of the proposed scientific experiment.

Table 6
Measured and predicted times of occurrence for selected impacts: a) in $\bar{\theta}_A(\bar{t})$, b) in $\bar{\theta}_B(\bar{t})$, c) in $\bar{\theta}_C(\bar{t})$ of the dual-clearance configuration (X1-2) given step excitation.

	Time of occurrence (normalized) for impact number					
	1st	2nd	5th	6th	9th	10th
a) $\bar{\theta}_A(\bar{t})$						
Measurement	0.33	0.87	2.58	3.16	5.05	5.73
Prediction	0.31	0.83	2.39	2.91	4.49	5.03
b) $\bar{\theta}_B(\bar{t})$						
Measurement	0.32	0.87	2.59	3.16	5.05	5.72
Prediction	0.31	0.83	2.39	2.91	4.49	5.03
c) $\bar{\theta}_C(\bar{t})$						
Measurement	0.34	0.90	2.61	3.21	5.09	5.81
Prediction	0.31	0.83	2.39	2.91	4.49	5.02

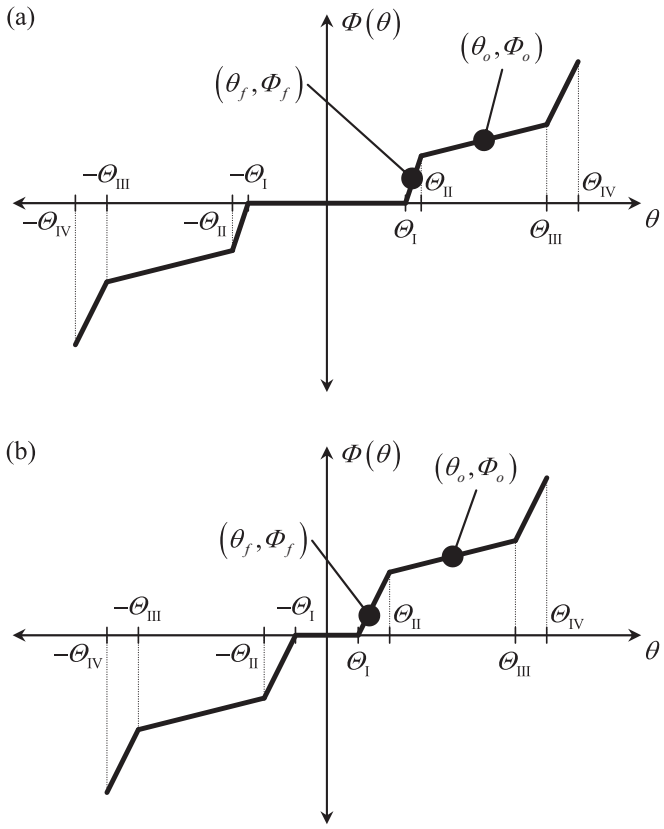

Fig. 12. Characteristics of two multi-staged clutch dampers (denoted C1 and C2) that are utilized in a prior large-scale experiment (denoted X2) [8]: a) C1 (where stage I is a very compliant spring); and b) C2 (where stage I is a spline clearance). Here, $\Phi(\theta)$ is the elastic torque transmission; see Fig. 1 for other symbols.

7. Conclusions

The chief contribution of this article is a new scientific experiment that exhibits the step-response of a torsional system that contains one or two controlled clearance non-linearities (single or dual-clearance configurations). Although it is similar in several aspects to large-scale experiments proposed in prior work [4–8], this new experiment is quite unique since it contains only well-known and controlled non-linear features while intentionally designed to be scaled ("bench-top"). Typical measurements (for both the single and dual-clearance configurations) exhibit richly non-linear behavior, including

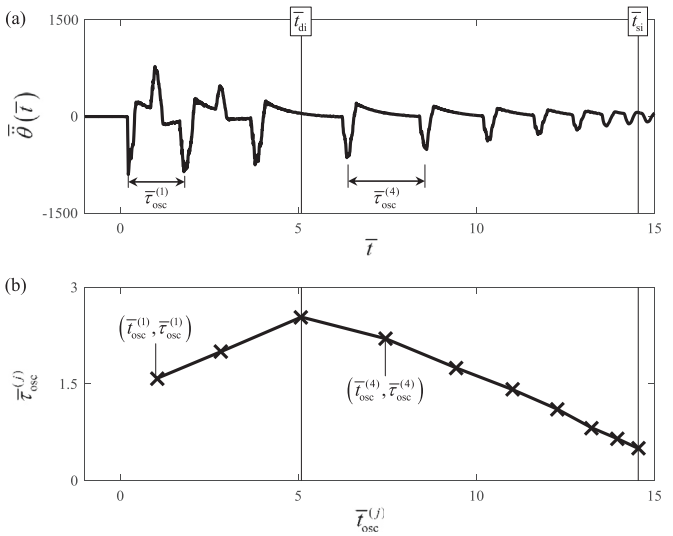

Fig. 13. Measured step-response of clutch damper C1 (X2-C2) from the prior experiment X2 [8] with: a) angular acceleration $\ddot{\bar{\theta}}(\bar{t})$; and b) impulse period $\bar{\tau}_{osc}^{(j)}$ (for double (di) and single-sided (si) impact regimes only). Here, $\bar{t}_{di}$ is the time of transition from double to single-sided impact regimes and $\bar{t}_{si}$ is the time of transition from the single to no-impact regime. Key: (▬▬) – $\ddot{\bar{\theta}}(\bar{t})$ and (▬x▬) – $\bar{\tau}_{osc}^{(j)}$.

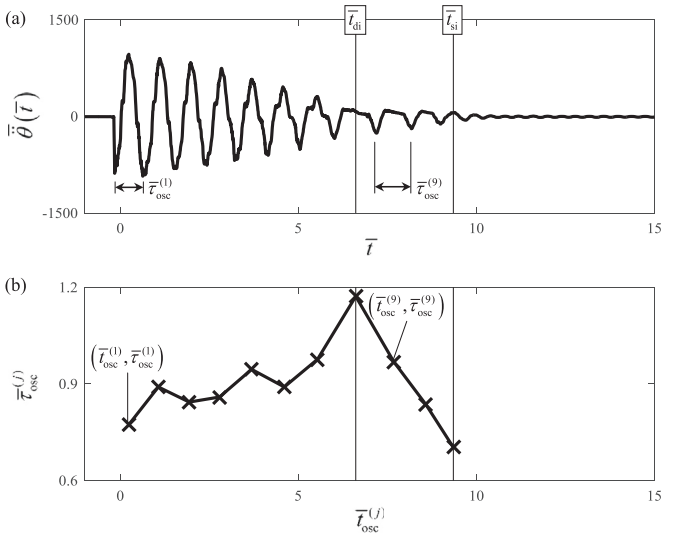

Fig. 14. Measured step-response of clutch damper C2 (X2-C2) from the prior experiment [8] with: a) angular acceleration $\ddot{\bar{\theta}}(\bar{t})$; and b) impulse period $\bar{\tau}_{osc}^{(j)}$ (for double (di) and single-sided (si) impact regimes only). Here, $\bar{t}_{di}$ is the time of transition from double to single-sided impact regimes and $\bar{t}_{si}$ is the time of transition from the single to no-impact regime. Key: (▬▬) – $\ddot{\bar{\theta}}(\bar{t})$ and (▬x▬) – $\bar{\tau}_{osc}^{(j)}$.

the double-sided impact regime [8,9] and a time-varying oscillatory period. Reasonable agreement between the measurements and predictions from simplified, reduced-order non-linear models verify that the experiment (in various configurations) operates as intended. However, it is also obvious that more refined higher-dimensional non-linear models are necessary to better describe the physics of the system. A qualitative comparison to a prior large-scale experiment [8] demonstrates the relevance and applicability to the literature [4–8]. Further, a redesign of the proposed experiment could enhance its utility. For example, introducing asymmetry to the torsion arm would migrate the final operating point $(\theta_{AB\_f}, \Phi_{AB\_f})$ towards an angular transition $\pm\Theta_{AB\_1}$, thus increasing the likelihood of the single-sided impact regime (si). Finally, the proposed scientific experiment should yield critical time domain benchmark data that is collected under laboratory conditions with well-known and controlled features. This dataset is essential for the validation of non-linear simulation models, parameter estimation [11], as well as providing insight into the role of one or multiple clearance non-linearities within a torsional system.

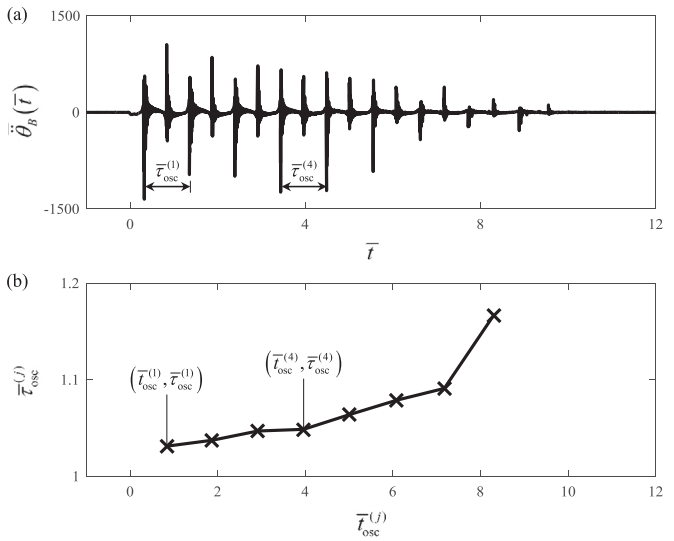

Fig. 15. Measured step-response of the single-clearance configuration (X1-1a) of the proposed experiment: a) angular acceleration $\ddot{\bar{\theta}}_B(\bar{t})$; and b) impulse period $\bar{\tau}_{osc}^{(j)}$. Key: (▬▬) – $\ddot{\bar{\theta}}_B(\bar{t})$ and (▬x▬) – $\bar{\tau}_{osc}^{(j)}$.

Acknowledgment

The authors acknowledge Eaton Corporation (Clutch Division) for supporting this research. We would like to thank Luiz Pereira and Brian Franke for their assistance with experimental studies. Further, we acknowledge the member organizations of the Smart Vehicle Concepts Center (www.SmartVehicleCenter.org) and the National Science Foundation.

Appendix A. List of symbols

Symbols

E	Young's modulus
h	Coulomb friction coefficient
I	area moment of inertia
J	torsional inertia
k	torsional stiffness
L	translational distance (length)
$\ddot{q}$	translational acceleration
R	radius
t	time
T	external torque
β	wave number
γ	mass per unit length
Δ	finite change
η	regularizing factor for Coulomb friction
$\theta, \dot{\theta}, \ddot{\theta}$	angular displacement, velocity, and acceleration
Θ	stage transition (angular)
ρ	material density
τ	oscillatory period
Φ	elastic torque transmission
Ξ	unit-step function
ω	circular frequency

Subscripts

A, B, C	absolute coordinate and element indices

AB, *BC*	relative coordinate and element indices
arm	torsion arm
di	double-sided impact
disk	disk
f	final point
imp	impulse
I, II, ...	stage index
gap	gap or clearance
max	maximum
n	natural
ni	no-impact
o	initial point
osc	oscillatory
probe	translational displacement probe
r	modal index
shaft	shaft
si	single-sided impact
stick	sticking condition (dry friction)
x, *y*, *z*	spatial indices (length, width, thickness)
μ	average

Abbreviations

1,2,3DOF	one, two, and three degree(s) of freedom
X1-0	proposed experiment, no-clearance configuration
X1-1a,b	proposed experiment, single-clearance configuration(s)
X1-2	proposed experiment, dual-clearance configuration
X1-P1,2,3	proposed sub-experiments for parameter estimation
X2	prior large-scale experiment (see Ref. [8])

Appendix B. List of instrumentation

Craftsman Digital Torpedo Level [17]:

- Measurement range: 0–360°
- Accuracy of digital display: $\pm 0.1°$
- Accuracy of vials: $\pm 0.029°$

PCB translational accelerometer model 355B02 [18]:

- Sensitivity: 10 mV/g
- Measurement range: ± 500 g (peak)
- Frequency range for $\pm 5\%$ accuracy: 1–10,000 Hz
- Frequency range for $\pm 10\%$ accuracy: 0.6–12,000 Hz
- Frequency range for ± 3 dB accuracy: 0.3–17,000 Hz
- Resonant frequency: ≥ 35 kHz
- Broadband amplitude resolution (1–10,000 Hz): 0.0005 g RMS

National Instruments analog input module model NI 9234 [19]:

- Sampling frequency: 51.2 kHz per channel
- Voltage range: ± 5 V
- Digital resolution: 24-bit
- Dynamic range: 102 dB
- Anti-aliasing filters

OMEGA translational displacement transducer Model LD500-2.5 [22]:

- Stroke: ± 2.5 mm
- Spring rate: 13 g/mm
- Voltage range: ± 10 V
- Sensitivity: 73.31 mV/V/mm

References

[1] J.P. Den Hartog, Mechanical Vibrations, 4th ed. McGraw-Hill, New York, 1956.
[2] R.A. Ibrahim, Recent advances in nonlinear passive vibration isolators, J. Sound. Vib. 314 (2008) 371–452, http://dx.doi.org/10.1016/j.jsv.2008.01.014.
[3] F. Shaver, Manual Transmission Clutch Systems, SAE (1997).
[4] Ph Couderc, J. Callenaere, J. Der Hagopian, G. Ferraris, A. Kassai, Y. Borjesson, L. Verdillon, S. Gairmard, Vehicle driveline dynamic behavior: experimentation and simulation, J. Sound. Vib. 218 (1998) 133–157, http://dx.doi.org/10.1006/jsvi.1998.1808.
[5] J.W. Biermann, B. Hagerodt, Investigation of the clonk phenomenon in vehicle transmissions – measurement, modelling, and simulation, Proc. IMechE Part K: J. Multi-body Dyn. 213 (1999) 53–60, http://dx.doi.org/10.1243/1464419991544054.
[6] M.T. Menday, H. Rahnejat, M. Ebrahimi, Clonk: an onomatopoeic response in torsional impact of automotive drivelines, Proc. IMechE. Part D: J. Automob. Eng. 213 (1999) 349–357, http://dx.doi.org/10.1243/0954407991526919.
[7] A.R. Crowther, R. Singh, N. Zhang, C. Chapman, Impulsive response of an automatic transmission system with multiple clearances: formulation, simulation, and experiment, J. Sound. Vib. 306 (2007) 444–466.
[8] M.D. Krak, J.T. Dreyer, R. Singh, Step-response of a torsional device with multiple discontinuous non-linearities: formulation of a vibratory experiment, Mech. Syst. Signal Process. 70–71 (2016) 1117–1130, http://dx.doi.org/10.1016/j.ymssp.2015.08.013.
[9] R.J. Comparin, R. Singh, An analytical study of automotive neutral gear rattle, ASME J. Mech. Des. 112 (1990) 237–245.
[10] T.E. Rook, R. Singh, Dynamic analysis of a reverse-idler gear pair with concurrent clearances, J. Sound. Vib. 182 (1995) 303–322, http://dx.doi.org/10.1006/jsvi.1994.0198.
[11] G. Kerschen, K. Worden, A.F. Vakakis, J.C. Golinval, Past, present and future of nonlinear system identification in structural dynamics, Mech. Syst. Signal Process. 20 (2006) 505–592, http://dx.doi.org/10.1016/j.ymssp.2005.04.008.
[12] T.C. Kim, T.E. Rook, R. Singh, Effect of smoothening function on the frequency response of an oscillator with clearance non-linearity, J. Sound. Vib. 263 (2003) 665–678.
[13] D.T. Greenwood, Principles of Dynamics, Prentice-Hall, Upper Saddle River, New Jersey, 1988.
[14] Jaw Type Couplings, Lovejoy. ⟨http://www.lovejoy-inc.com⟩, (accessed January 2016).
[15] L. Meirovitch, Fundamentals of Vibrations, Waveland Press, Inc., Long Grove, Illinoise, 2010.
[16] Solidworks, Dassault Systemes. ⟨http://www.solidworks.com⟩, (accessed January 2016).
[17] ANSYS. ⟨http://www.ansys.com⟩, (accessed January 2016).
[18] Craftsman Digital Torpedo Level. ⟨http://www.sears.com⟩, (accessed January 2016).
[19] Translational Accelerometer, Model 355B02, PCB Piezotronics Inc. ⟨http://www.pcb.com⟩, (Accessed March 2015).
[20] Data Acquisition System, Model NI cDAQ-9184, National Instruments. ⟨http://sine.ni.com⟩, (accessed January 2016).
[21] Analog Input Module, Model NI 923, National Instruments. ⟨http://sine.ni.com⟩, (accessed February 2016).
[22] LabVIEW System Design Software, National Instruments. ⟨http://www.ni.com⟩, (accessed January 2016).
[23] Translational displacement transducer, Model LD500−2.5, OMEGA. ⟨http://www.omega.com⟩, (accessed February 2016).
[24] MATLAB, MathWorks. ⟨http://www.mathworks.com/products/matlab/⟩, (Accessed January 2016).